[Proceeding] Osmotic phenomena in bentonites

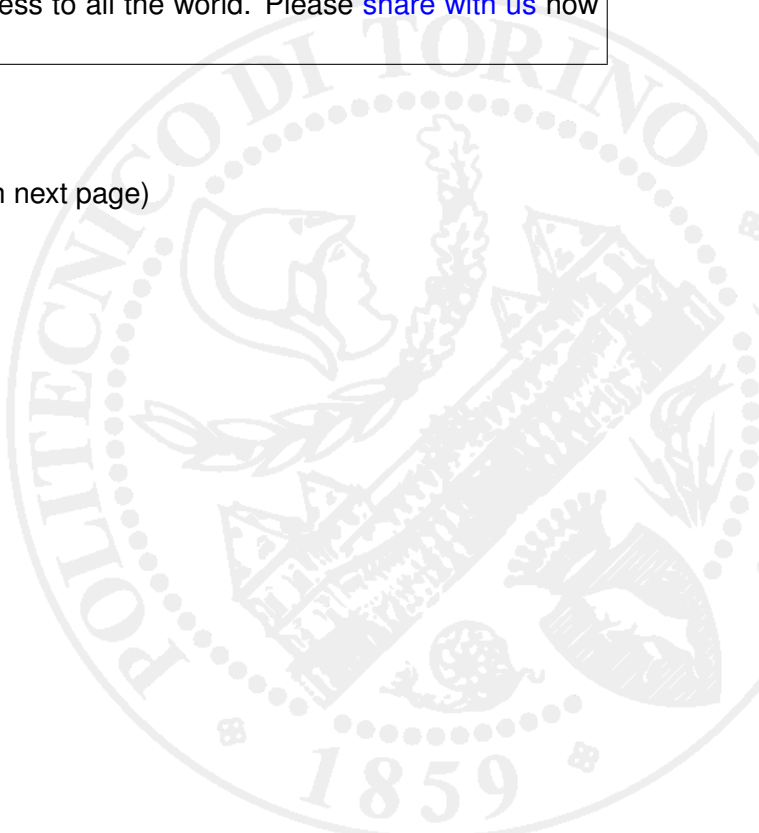

Osmotic phenomena in bentonites

A. Dominijanni, M. Manassero & S. Puma
Politecnico di Torino, Italy

ABSTRACT: A theoretical approach has been proposed in order to derive constitutive equations for the coupled chemical-hydraulic-mechanical behaviour of bentonites, which are clay soils characterized by a high specific surface and a permanent negative electric charge on their solid skeleton. The phenomenological parameters that govern the transport of electrolyte solutions through bentonites, i.e. the reflection coefficient, which is also called the chemico-osmotic efficiency coefficient, and the osmotic effective diffusion coefficient, have been measured through laboratory tests on a sodium bentonite with porosity of 0.81, over a range of sodium chloride concentrations in the pore solution that varied from 5 mM to 100 mM. The relevance of the osmotic phenomena has been shown to decrease when the salt concentration increases for this bentonite. The reflection coefficient has been measured also on a calcium bentonite, over a range of calcium chloride concentrations in the pore solution that varied from 5 mM to 10 mM: in this case, the osmotic behaviour has resulted to be negligible. The obtained results have been interpreted by assuming that the microscopic deviations of the pore solution state variables from their average values are negligible. In this way, it has been possible to interpret the macroscopic behaviour on the basis of the physical and chemical properties of the bentonite mineralogical components.

1 INTRODUCTION

The term "bentonite" is commonly used to indicate a clay soil with a high content (> 70%) of montmorillonite, a mineral of the smectite group. Montmorillonite particles are thin lamellae that are characterized by a high specific surface (defined as the surface per unit weight) and a permanent negative electric charge. Bentonite is used in hydraulic and contaminant barriers, because of its low hydraulic conductivity, k, to permeation with water and dilute aqueous solutions (k typically $\leq 3 \cdot 10^{-11}$ m/s). Geosynthetic clay liners (GCLs), which consist of a thin layer of bentonite (~ 5- to 10-mm thick) sandwiched between two geotextiles, are examples of such barriers. GCLs are currently used in bottom and cover landfill barriers to limit water infiltration and contaminant migration.

Owing to its physical and chemical properties, the macroscopic mechanical behaviour and transport properties of bentonite cannot be modelled through classical soil mechanics approaches. In fact, bentonite swells or shrinks in response to changes in the chemical composition of the pore solution. Moreover, when a hydraulic pressure gradient, or a solute concentration gradient, is applied to it, both a volumetric flux and a diffusive solute mass flux occur, as in semipermeable membranes. For this reason, a theoretical approach that accounts for the electric interaction that occurs between the solid skeleton of the bentonite and the ions contained in the pore solution is proposed in the first part of this paper. The experimental determination of the swelling pressure and the transport properties of both a natural sodium bentonite and a calcium bentonite is described in the second part. The obtained results have been interpreted with the proposed theoretical model, in which the microscopic properties of the bentonite have been linked to the observed macroscopic behaviour.

2 THEORY

Montmorillonite lamellae are characterized by a negative electric charge, due to the isomorphic substitution of a portion of the tetravalent silicon (Si^{4+}) and the trivalent aluminium (Al^{3+}) in their crystalline structure, with metals, such as magnesium (Mg^{2+}), which have a lower valence. This electric charge per unit solid volume can be expressed as $F \cdot \bar{c}_{sk,0}$, where F is Faraday's constant (96,485 $C \cdot mol^{-1}$) and $\bar{c}_{sk,0}$ is the molar concentration per unit solid volume of the solid skeleton electric charge, which is assumed to have unit valence (i.e. $z_{sk} = -1$). $\bar{c}_{sk,0}$ represents the moles of solid skeleton electric charge per volume of solids and, in order to be compared with the

ion concentrations of the pore solution, it needs to be divided by the void ratio, e, which represents the pore volume per volume of solids. Dominijanni and Manassero (2012b) have shown that $\bar{c}_{sk,0}$ is proportional to the effective specific surface of the solid particles and decreases when the montmorillonite lamellae aggregate to form the so-called tactoids.

If the pore solution contains a single salt that is completely dissociated with the following stoichiometric reaction:

$$(\text{Cation})_{z_1}^{\nu_1}(\text{Anion})_{z_2}^{\nu_2} \rightarrow \nu_1(\text{Cation})^{z_1} + \nu_2(\text{Anion})^{z_2}$$

where z_1 and z_2 are the electrochemical valences of the cation and the anion, and ν_1 and ν_2 are the stoichiometric coefficients of the cation and the anion, respectively, the following condition has to be satisfied in order to preserve electroneutrality within a saturated porous medium, even in the presence of the solid skeleton electric charge:

$$z_1\bar{c}_1 + z_2\bar{c}_2 = \frac{\bar{c}_{sk,0}}{e} \tag{1}$$

where $\bar{c}_1$ and $\bar{c}_2$ are the molar concentrations of the cation and the anion, respectively, and e is the void ratio.

As a consequence, the solid skeleton electric charge influences the distribution of the ions contained in the pore solution. This phenomenon is known as the ion-partition effect and is expected to be more relevant for porous media characterized by higher solid skeleton charge concentrations.

2.1 *Equilibrium conditions*

When an electrically charged porous medium is placed in contact with an external bulk solution that contains the same ions that are present in the pore solution, a thermodynamic equilibrium condition is reached, after a certain period of time, in which the water chemical potential and the ion electrochemical potentials between the two solutions are equal. The external bulk solution can be considered as a "chemical thermometer" in order to evaluate the equilibrium conditions of the porous medium (Coussy, 2004). The electroneutrality condition in the external solution is given by:

$$z_1c_1 + z_2c_2 = 0 \tag{2}$$

where c_1 and c_2 are the molar concentrations of the cation and the anion that are contained in the bulk solution.

It is convenient to define the salt concentration, c_s, of the external solution as follows:

$$c_s = \frac{c_1}{\nu_1} = \frac{c_2}{\nu_2} \tag{3}$$

Using Eq. (3), the electroneutrality condition, Eq. (2), provides the relation between the electrochemical valences and the stoichiometric coefficients:

$$z_1\nu_1 + z_2\nu_2 = 0\,. \tag{4}$$

As a result, the equilibrium condition can be characterized by the following state variables of the external bulk solution: the absolute temperature, T, the hydraulic pressure (referenced to the atmospheric pressure, as is usual in soil mechanics), u, and the salt concentration, c_s. The corresponding variables of the pore solution can be evaluated from the following conditions:

$$\bar{T} = T \tag{5}$$

$$\bar{\mu}_w = \mu_w \tag{6}$$

$$\bar{\mu}_i^{ec} = \mu_i^{ec} \qquad i = 1,2 \tag{7}$$

where $\bar{T}$ and T are the absolute temperature in the pore solution and in the external bulk solution, respectively; $\bar{\mu}_w$ and μ_w are the water chemical potential in the pore solution and in the external bulk solution, respectively; $\bar{\mu}_i^{ec}$ and μ_i^{ec} are the electrochemical potentials of the i-th ion in the pore solution and in the external bulk solution, respectively.

The water chemical potential, μ_w, and the ion electrochemical potentials, μ_i^{ec}, of the external solution can be related to the hydraulic pressure, u, and the salt concentration, c_s, for a dilute solution, as follows (Katchalsky and Curran, 1965; Dominijanni and Manassero, 2012a):

$$\mu_w = \mu_w^0(T) + \frac{(u - \Pi)}{c_w} \tag{8}$$

$$\begin{aligned}\mu_i^{ec} &= \mu_i + z_iF\varphi = \\ &= \mu_i^0(T) + RT\ln(\nu_i c_s) + z_iF\varphi \quad i = 1,2\end{aligned} \tag{9}$$

where μ_w^0 and μ_i^0 are integration constants that only depend on the absolute temperature T; c_w is the water molar concentration; $\Pi = RT\sum_{i=1}^{2}\nu_i c_s$ is the osmotic pressure; μ_i is the chemical potential of the i-th ion; R is the universal gas constant ($8.314\ \text{J}\cdot\text{mol}^{-1}\cdot\text{K}^{-1}$); and φ is the electric potential.

The state variables in the external bulk solution can be measured easily, whereas it is very difficult to determine the corresponding variables in the pore solution. Moreover, the relations obtained by linking

the chemical potentials to the state variables of the pore solution are more uncertain, due to the interaction with the solid skeleton charge, which alters the ion concentration distribution near the solid particles. The simplest assumption that can be adopted involves using analogous relations to Eqs. (8) and (9), as they are also considered valid for the pore solution. This assumption, which was first proposed by Donnan (1911), neglects the microscopic deviations of the ion concentrations from their average values that are induced by the electric potential distribution within the pores. If this approximation is accepted, the water chemical potential, $\bar{\mu}_w$, and the ion electrochemical potentials, $\bar{\mu}_i^{ec}$, of the pore solution can be expressed as follows:

$$\bar{\mu}_w = \bar{\mu}_w^0(T) + \frac{(\bar{u} - \bar{\Pi})}{\bar{c}_w} \tag{10}$$

$$\begin{aligned} &\bar{\mu}_i^{ec} = \bar{\mu}_i + z_i F\bar{\varphi} = \\ &= \bar{\mu}_i^0(T) + RT\ln(\bar{c}_i) + z_i F\bar{\varphi} \qquad i = 1,2 \end{aligned} \tag{11}$$

where $\bar{\mu}_w^0$ and $\bar{\mu}_i^0$ are integration constants that only depend on the absolute temperature T; $\bar{c}_w$ is the molar concentration of the water in the pore solution, which can be taken equal to the molar concentration of the water in the external bulk solution, i.e. $\bar{c}_w \cong c_w$; $\bar{\Pi} = RT\sum_{i=1}^{2}\bar{c}_i$ is the osmotic pressure of the pore solution; $\bar{\mu}_i$ is the chemical potential of the i-th ion in the pore solution; and $\bar{\varphi}$ is the electric potential in the pore solution.

The hydraulic pressure of the pore solution, $\bar{u}$, and the ion partition factors, Γ_i, defined as the ratio between the ion concentration of the pore solution and the ion concentration of the external bulk solution, can therefore be expressed on the basis of Eqs. (6) and (7), and using Eqs. (8)-(11), as follows:

$$\bar{u} = u + (\bar{\Pi} - \Pi) \tag{12}$$

$$\Gamma_i = \frac{\bar{c}_i}{c_i} = \frac{\bar{c}_i}{\nu_i c_s} = \exp\left(-z_i \frac{F}{RT}\bar{\psi}\right) \qquad i = 1,2 \tag{13}$$

where $\bar{\psi} = \bar{\varphi} - \varphi$ is the electric potential of the porous medium, which is also called Donnan's potential.

On the basis of this approach, the hydraulic pressure of the pore solution is different from the hydraulic pressure of the external solution that is in equilibrium with it. The pressure difference between the pore solution and the external solution is called the swelling pressure, u_{sw}, and is given by:

$$u_{sw} = \bar{\Pi} - \Pi . \tag{14}$$

Eqs. (12) and (13) for $i = 1,2$, together with Eq. (1), constitute a set of four equations that can be solved to find the four unknown variables: the hydraulic pressure, $\bar{u}$, the ion concentrations, $\bar{c}_i$ for $i = 1,2$, and the electric potential, $\bar{\psi}$.

When the ion electrochemical valences are both unitary, such as for NaCl, Eq. (13) implies that

$$\Gamma_1 = \Gamma_2^{-1} . \tag{15}$$

Inserting Eq. (15) into Eq. (1) results in the following equation:

$$\Gamma_2^{-1} - \Gamma_2 - \frac{\bar{c}_{sk,0}}{e \cdot c_s} = 0 , \tag{16}$$

which has a positive solution of the following form:

$$\Gamma_2 = -\frac{\bar{c}_{sk,0}}{2 \cdot e \cdot c_s} + \sqrt{\left(\frac{\bar{c}_{sk,0}}{2 \cdot e \cdot c_s}\right)^2 + 1} \tag{17}$$

$$\Gamma_1 = \Gamma_2^{-1} = \frac{\bar{c}_{sk,0}}{2 \cdot e \cdot c_s} + \sqrt{\left(\frac{\bar{c}_{sk,0}}{2 \cdot e \cdot c_s}\right)^2 + 1} . \tag{18}$$

On the basis of Eqs. (17) and (18), the swelling pressure can be expressed as follows:

$$\begin{aligned} u_{sw} &= RTc_s\left(\Gamma_1 + \Gamma_2 - 2\right) = \\ &= 2RTc_s\left[\sqrt{\left(\frac{\bar{c}_{sk,0}}{2 \cdot e \cdot c_s}\right)^2 + 1} - 1\right] . \end{aligned} \tag{19}$$

2.2 *Transport equations*

The most general approach for modelling coupled fluxes is to invoke phenomenological equations by applying the formalism of the Thermodynamics of Irreversible Processes (Katchalsky and Curran, 1965; Yaroshchuk, 1995; Dominijanni and Manassero, 2012a,b). The main advantage of this approach is to avoid any specification of physical properties of the membrane, maintaining the model as general as possible. Using such a formalism, Dominijanni et al. (2013) derived the following equations for the volumetric flux, q, and the salt flux, J_s, for a semipermeable porous medium permeated by a solution containing a single salt (e.g. NaCl or $CaCl_2$):

$$q = -\frac{k}{\gamma_w}\left(\frac{\partial u}{\partial x} - \omega\frac{\partial \Pi}{\partial x}\right) \tag{20}$$

$$J_s = (1-\omega)qc_s - nD_\omega^* \frac{\partial c_s}{\partial x} \tag{21}$$

where

$$k = \frac{n \cdot \gamma_w}{\alpha\left[1 + \frac{RT}{\alpha}\frac{(\Gamma_1 - \Gamma_2)^2 \nu_1 \nu_2 c_s}{\nu_1 \Gamma_2 D_2 + \nu_2 \Gamma_1 D_1}\right]} \quad (22)$$

$$\omega = 1 - \frac{\nu_1 D_2 + \nu_2 D_1}{\nu_1 \Gamma_2 D_2 + \nu_2 \Gamma_1 D_1}\Gamma_1 \Gamma_2 \quad (23)$$

$$D^*_\omega = (1-\omega) \cdot D_s \quad (24)$$

$$D_s = \frac{(\nu_1 + \nu_2) D_1 D_2}{\nu_1 D_2 + \nu_2 D_1}. \quad (25)$$

In Eqs. (20)-(25), k is the hydraulic conductivity, n is the porosity, γ_w is the water unit weight, α is the hydraulic friction coefficient, ω is the reflection coefficient, D_i is the macroscopic diffusion coefficient of the i-th ion and D^*_ω is the osmotic effective diffusion coefficient.

Dominijanni and Manassero (2012b) have demonstrated that, if the microscopic deviations of the variables from their average values are assumed to be negligible, the macroscopic ion diffusion coefficients, D_i, result to be equal to the ion effective diffusion coefficients, D^*_i:

$$D_i = D^*_i = \tau_m D_{i,0} \qquad i = 1,2 \quad (26)$$

$$D_s = D^*_s = \frac{(\nu_1 + \nu_2) D^*_1 D^*_2}{\nu_1 D^*_2 + \nu_2 D^*_1} = \\ = \tau_m \frac{(\nu_1 + \nu_2) D_{1,0} D_{2,0}}{\nu_1 D_{2,0} + \nu_2 D_{1,0}} = \tau_m D_{s,0} \quad (27)$$

where τ_m is the dimensionless matrix tortuosity factor that accounts for the tortuous nature of the actual diffusive pathway through the porous medium (Malusis and ShacKelford, 2002b), $D_{i,0}$ is the free (aqueous) solution diffusion coefficient of the i-th ion, D^*_s is the salt effective diffusion coefficient and $D_{s,0}$ is the free solution diffusion coefficient of the salt. When the solid skeleton electric charge is equal to zero, the ion partition coefficients, Γ_i, are equal to 1 and Eqs. (20) and (21) reduce to the Darcy equation and the classical advective-diffusion equation, respectively.

The osmotic effective diffusion coefficient, D^*_ω, results to be related to the reflection coefficient, ω, through Eq. (24), so that $D^*_\omega = 0$ when $\omega = 1$. As a result, the condition $\omega = 1$ implies a null salt flux through the porous medium, which, in this case, can

The coefficient k can be measured, under steady state conditions, using traditional permeameters. Malusis et al. (2001) developed a testing apparatus to determine ω and D^*_ω. This apparatus is able to impose the condition of no-volumetric flux (q = 0) through a soil sample in contact with two external solutions, maintained at constant salt concentrations, so that the global or averaged values of the coefficients can be measured. The global values of ω and D^*_ω are defined as follows:

$$\omega_g = \frac{1}{\Delta c_s}\int_{c_b}^{c_t} \omega \cdot dc_s \quad (28)$$

$$D^*_{\omega g} = \frac{1}{\Delta c_s}\int_{c_b}^{c_t} D^*_\omega \cdot dc_s \quad (29)$$

where c_t and c_b represent the salt concentration at the top and the bottom boundaries of the clay sample, respectively, and $\Delta c_s = c_t - c_b$ is their difference. These coefficients can be determined by means of the following relations under steady state conditions:

$$\omega_g = \left(\frac{\Delta u}{\Delta \Pi}\right)_{q=0} \quad (30)$$

$$D^*_{\omega g} = \frac{L}{n}\left(\frac{J_s}{\Delta c_s}\right)_{q=0} \quad (31)$$

where $\Delta u = u_t - u_b$ and $\Delta \Pi = \Pi_t - \Pi_b$ represent the differences between the hydraulic pressure and the osmotic pressure at the boundaries of the clay sample, and L is the length of the sample.

It is interesting to observe that the relationship between D^*_ω and ω is also maintained between their corresponding global values: in fact, inserting Eq. (24) into Eq. (29) with $D_s = D^*_s$ leads to:

$$D^*_{\omega g} = (1-\omega_g) \cdot D^*_s = (1-\omega_g) \cdot \tau_m \cdot D_{s,0}. \quad (32)$$

In the case of a salt constituted by monovalent ions, inserting Eq. (23) into Eq. (28) and using Eqs. (17) and (18), the following expression of ω_g is obtained:

$$\omega_g = 1 + \frac{\bar{c}_{sk,0}}{2 \cdot \Delta c_s \cdot e}\left[Z_2 - Z_1 - (2t_1 - 1) \cdot \ln\left(\frac{Z_2 + 2t_1 - 1}{Z_1 + 2t_1 - 1}\right)\right] \quad (33)$$

where

$$t_1 = \frac{D_{1,0}}{D_{1,0} + D_{2,0}} = \text{cation transport number}, \quad (34)$$

$$Z_1 = \sqrt{1 + \left(\frac{2 \cdot c_t \cdot e}{\bar{c}_{sk,0}}\right)^2}, \quad (35)$$

$$Z_2 = \sqrt{1 + \left(\frac{2 \cdot c_b \cdot e}{\bar{c}_{sk,0}}\right)^2}. \quad (36)$$

3 MATERIALS AND METHODS

3.1 *Materials*

The powdered bentonite tested in this study is an Indian sodium bentonite that is used for the production of a needle-punched GCL. The bentonite is characterized by a cation exchange capacity (CEC, measured using the methylene blue adsorption method) of 105 meq/100g. The mineralogical composition, evaluated through x-ray diffraction analysis, indicates a bentonite that is primarily composed of smectite (> 98%) with traces of calcite, quartz, mica and gypsum.

The bentonite is characterized by a liquid limit (LL) of 525% and a hydraulic conductivity of 8·10-12 m/s, measured at a 27.5 kPa confining effective stress using de-ionized water as the permeant liquid.

Sodium solutions were prepared with sodium chloride (ACS reagent, purity ≥ 99%) and de-ionized water (DW). The sodium solutions were prepared at different molarity values, in the 5 mM to 100 mM range, with the aim of investigating the effect of the monovalent cations on the osmotic behaviour of the bentonite. The DW (pH = 6.95; EC at 20 °C = 0.6 mS/m) consisted of tap water processed through a series of activated carbon filters, a reverse osmosis process and, finally, a UV lamp (Elix Water Purification system). Moreover, the DW was deaerated prior to use. The electrical conductivity (EC) measured at 20 °C for the NaCl solutions ranged from 60.5 mS/m to 1.1 mS/m.

3.1.1 *Calcium bentonite preparation*

Calcium bentonite has been obtained through an accelerated degradation of sodium bentonite that was promoted by the cation exchange of calcium for sodium. Sodium bentonite was kept in contact with a highly concentrated (1M) calcium chloride solution for a week. In this way, sodium bentonite exchanged sodium cations with calcium cations present in the equilibrium solution. Excess soluble calcium ions, contained in the exchanged calcium bentonite were successively removed by a series of hydration with de-ionized water and consolidation cycles. Calcium bentonite was left to consolidate in de-ionized water and, when complete settlement was reached, excess water was removed and the material was hydrated once again. This procedure was stopped when the electrical conductivity of the equilibrium solution was less than 70 mS/m.

3.1.2 *Salt removal pretreatment*

Prior to the osmotic property determination, the bentonite was submitted to a process with the aim of removing the soluble salts, mainly sodium, which are naturally present inside the material, due to its marine origin. The treatment prevents soluble salts from interfering with the determination of the osmotic properties.

Previous studies (Malusis et al., 2001; Malusis and Shackelford, 2002a, 2002b; Shackelford and Lee, 2003; Yeo et al., 2005; Kang and Shackelford, 2009; Di Emidio 2010) have used the '*flushing*' method to remove soluble salts. This method consists of an initial permeation phase, performed under back pressure, which requires a long period of time (i.e. from months to a year), because of the low bentonite hydraulic conductivity.

In this study, the '*squeezing*' method has been used with the aim of reducing the salt removal time. The '*squeezing*' method consists of a series of consecutive phases of powder bentonite hydration with DW, at a higher water content than the liquid limit, and drained consolidation, performed in a consolidometer under a maximum load of 500 kPa. Moreover, the drained solution is sampled daily and the EC is monitored to evaluate the soluble salt concentration in the bentonite pore water. After the '*squeezing*' process, the material is oven dried at 105 °C and pulverized once again. When a 5 L consolidometer is used, the above procedure can produce about 500 g of squeezed dry powder bentonite, characterized by a lower EC value than 50 mS/m, in 40-50 days. The specimens for the chemico-osmotic test are prepared by rehydrating the squeezed bentonite with DW at a lower water content than the liquid limit value and then by statically compacting the material in a compaction mould, while allowing the excess water to be released. Dry powder bentonite is required for the swelling pressure test.

3.2 *Testing apparatus and procedure*

3.2.1 *Chemico-osmotic test*

The testing apparatus used to measure the global reflection coefficient and the global osmotic effective diffusion coefficient is described in detail in Malusis et al. (2001). The main components of the apparatus include the osmotic cell, the flow-pump system, the pressure transducer, which is used to measure the differential pressure that develops across the specimen during the test, and the data acquisition system.

The cell consists of a modified rigid wall permeameter, in which the top piston and the bottom pedestal are equipped with three ports each: two enable the different solutions to circulate through the top (electrolyte solution) and the bottom (DW) porous stones with the aim of establishing a constant concentration gradient across the specimen. The third port is installed in both the top piston and the bottom pedestal to allow the differential pressure across the specimen to be measured.

The flow-pump system, which consists of a dual-carriage syringe pump and two stainless steel accumulators (Model 33 - Twin syringe pump, produced

by Harvard, Holliston, MA), prevents the volumetric flux through the specimen by simultaneously injecting into and withdrawing from the porous stones the same volume of solution. In order to obtain this result, the syringes have to move at the same rate.

The test was performed according to the procedure proposed by Malusius et al. (2001): a solution containing a known electrolyte concentration was circulated in the top porous stone, while DW was circulated in the bottom porous stone. The concentration difference across the specimen was maintained constant by continuously infusing the two liquids at the boundaries of the specimen.

Since the specimen was preliminary squeezed with DW to remove the soluble salts, the EC of the electrolyte solutions in the flux exiting from the porous stones at the steady state was induced solely by the contributions of Cl^- and Na^+ ions.

A calibration was performed and showed that the relation between the EC and solution molarity was linear over the examined concentration range both for NaCl and $CaCl_2$ solutions. As a consequence, the EC of the withdrawn fluxes (i.e. from the top and bottom porous stones, respectively) was monitored by sampling the solution contained in the pistons, and the electrolyte molar concentration was derived using a linear relation. Since the volumetric flux through the specimen was hindered, the global reflection coefficient could be calculated using Eq. (33).

The diffusive solute flux through the specimen was calculated for the n-th sampling interval as follows:

$$J_s^n = \frac{\sum_{m=1}^{n}\left(c_s^m \cdot \Delta V^m\right)}{A_S \cdot \Delta t^n} = \frac{\Delta Q^n}{\Delta t^n} \qquad (37)$$

where c_s^n is the solute molar concentration measured by sampling the solution coming out from the bottom porous stone, ΔV^m is the volume of the solution circulating in the porous stones in the Δt^m interval, A_S is the cross-section of the specimen and ΔQ^n is the cumulative salt molar mass per unit area that passed through the specimen. The global osmotic effective diffusion coefficient, $D^*_{\omega g}$, is calculated at the steady state as follows:

$$D^*_{\omega g} = \frac{\Delta Q}{\Delta t} \cdot \frac{L}{n \cdot \left(c_{t,avg} - c_{b,avg}\right)} \qquad (38)$$

where $c_{t,avg}$ and $c_{b,avg}$ are the average top and bottom salt concentrations, respectively.

3.2.2 *Swelling pressure test*

The swelling pressure apparatus primarily consists of a stainless steel oedometer cell, a NaCl solution supply tank that is placed above the pressure panel, a displacement transducer connected to the cell top piston, which is used to measure the axial strains of the specimen, a load cell and a data acquisition system.

The swelling pressure apparatus consists of a rigid cell that confines the sample (i.e. the oedometer), which allows access to the water through both porous stones. The cell is connected to a pressure panel that allows the specimen to be back-pressurized. The rigid piston above the upper porous stone is connected to the load cell, which measures the pressure that has to be applied in order to hinder the axial strain of the specimen.

The test procedure requires a known amount of dry material to be dusted inside the oedometer ring, the cell to be assembled and a NaCl solution to be supplied. The specimen, which is characterized by an initial dry height of 5 mm, is allowed to swell to 10 mm. The piston is then blocked, the sample is back-pressured and the steady state swelling pressure is recorded after a short transitional phase.

Since the bentonite that is initially dusted inside the oedometer is dry, the pressure increases for a number of days, during the hydration phase, and the steady state swelling pressure is reached when hydration has been completed.

4 RESULTS AND INTERPRETATION

4.1 *Chemico-osmotic test on sodium bentonite*

The first chemico-osmotic test was performed using the oven dried squeezed sodium bentonite, rehydrated with DW and then statically compacted, in a drained compaction mould, at a porosity, n, equal to 0.81 (e = 4.26). After the preparation phase, the 17 mm thick specimen was transferred to the cell for the osmotic test.

After assembling the cell, DW was circulated through the top piston and the bottom pedestal for two weeks in order to establish a steady baseline differential pressure, before a concentration gradient was applied to the specimen. A source concentration of NaCl then was injected into the top porous stone, while DW was continuously circulated in the bottom porous stone.

A multiple-stage chemico-osmotic test was performed by sequential circulation of chemical solutions containing 5.16, 10.27, 20.24, 51.94 and 109.31 mM NaCl concentrations at a constant flow rate of 0.05 mL/min.

The EC values of the salt mass fluxes withdrawn from the top and the bottom porous stones, measured during the testing stages, are shown in Fig. 1.

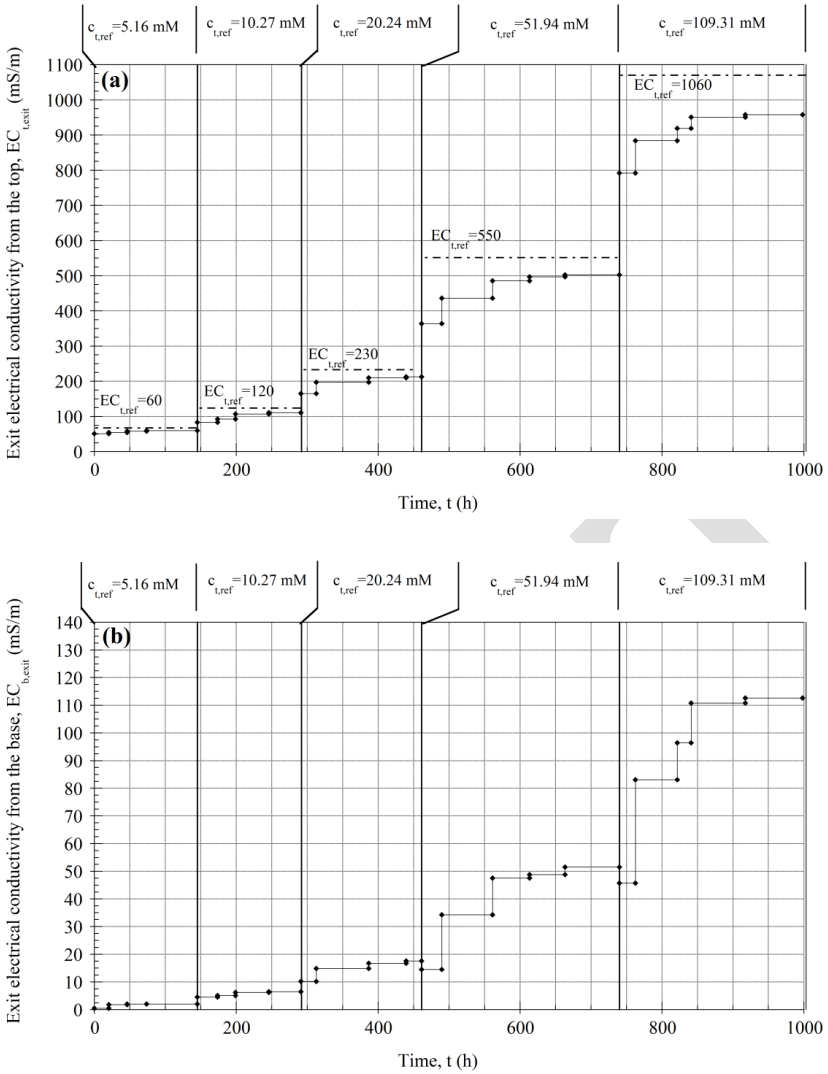

Figure 1. Electrical conductivity of the salt flux flux withdrawn from the top porous stone (a) and the bottom porous stone (b) as a function of time during the multiple-stage chemico-osmotic test on sodium bentonite.

The measured values depend on the NaCl concentrations imposed at the boundaries of the specimen: the EC values progressively increase during the test as the NaCl concentration of the injected solution in the top porous stone rises. The trends of the electrical conductivity of the flux withdrawn from the top porous stone, ECt,exit, and the electrical conductivity of the flux withdrawn from the bottom porous stone, ECb,exit, both show that a steady state has been reached for each stage.

Moreover, the difference between the EC values measured in the flux withdrawn from the top porous stone (ECt,exit) and the EC values of the solutions injected into the same stone (ECt,ref) is due to the loss in NaCl mass induced by the diffusion through the bentonite from the top to the bottom boundary.

The global reflection coefficient values, ω_g, obtained during the multiple-stage chemico-osmotic test, are shown in Fig. 2 as a function of time. The ω_g values are determined using Eq. (33), on the basis of the differential pressure, Δu, measured during the test with a time step of 10 min, and the osmotic pressure, $\Delta\Pi$, calculated from the average of the top and bottom NaCl concentrations. The steady state values of the variables are reported in Table 1 for each concentration stage.

As far as the EC measurements are concerned, the trend of the global reflection coefficient shows that a steady state has been reached for each stage. The steady state ω_g values tend to decrease as the salt concentration in the top porous stone increases. The recorded values range from 68%, for a 5.16 mM NaCl source concentration, to 5%, for a 109.31 mM NaCl source concentration. The global reflection coefficient can be assumed approximately null for higher molarities. The cumulative molar mass per unit area, Q, of the NaCl that migrated through the specimen during the multiple-stage test is reported in Fig. 3. The values of the global osmotic effective diffusion coefficient, $D^*_{\omega g}$, which have been obtained from the Q measurements shown in Fig. 3, are reported in Table 1.

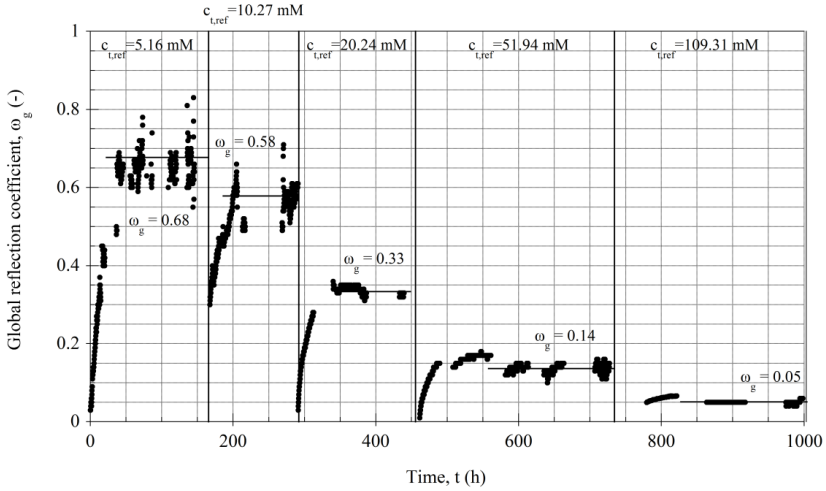

Figure 2. Global reflection coefficient as a function of time during the multiple-stage chemico-osmotic test.

Table 1 - Steady state values of the variables involved in the multiple-stage chemico-osmotic test, where: $c_{t,exit}$ and $c_{b,exit}$ are the NaCl concentrations of the flux withdrawn from the top and the bottom porous stones, respectively; $c_{t,avg}$ and $c_{b,avg}$ are the NaCl average concentrations in the top and the bottom porous stones, respectively; Δu is the hydraulic pressure difference between the top and the bottom specimen boundaries, measured by the differential transducer; $\Delta\Pi$ is the osmotic pressure difference; ω_g is the global reflection coefficient and $D^*_{\omega g}$ is the global osmotic effective diffusion coefficient.

$c_{t,ref}$	$c_{t,exit}$ (mM)	$c_{b,exit}$ (mM)	$c_{t,avg}$ (mM)	$c_{b,avg}$ (mM)	Δu (kPa)	$\Delta\Pi$ (kPa)	ω_g (-)	$D^*_{\omega g}$ (m^2/s)
5.16 mM	5.12	0.83	5.14	0.42	15.65	23.02	0.68	-
10.27 mM	9.61	0.85	9.94	0.43	26,87	46.33	0.58	$2.54 \cdot 10^{-10}$
20.24 mM	18.93	1.45	19.58	0.72	30.32	91.89	0.33	$3.52 \cdot 10^{-10}$
51.94 mM	47.39	4.39	49.67	2.19	32.38	231.30	0.14	$4.19 \cdot 10^{-10}$
109.31 mM	97.18	9.78	103.24	4.89	23.96	479.21	0.05	$4.60 \cdot 10^{-10}$

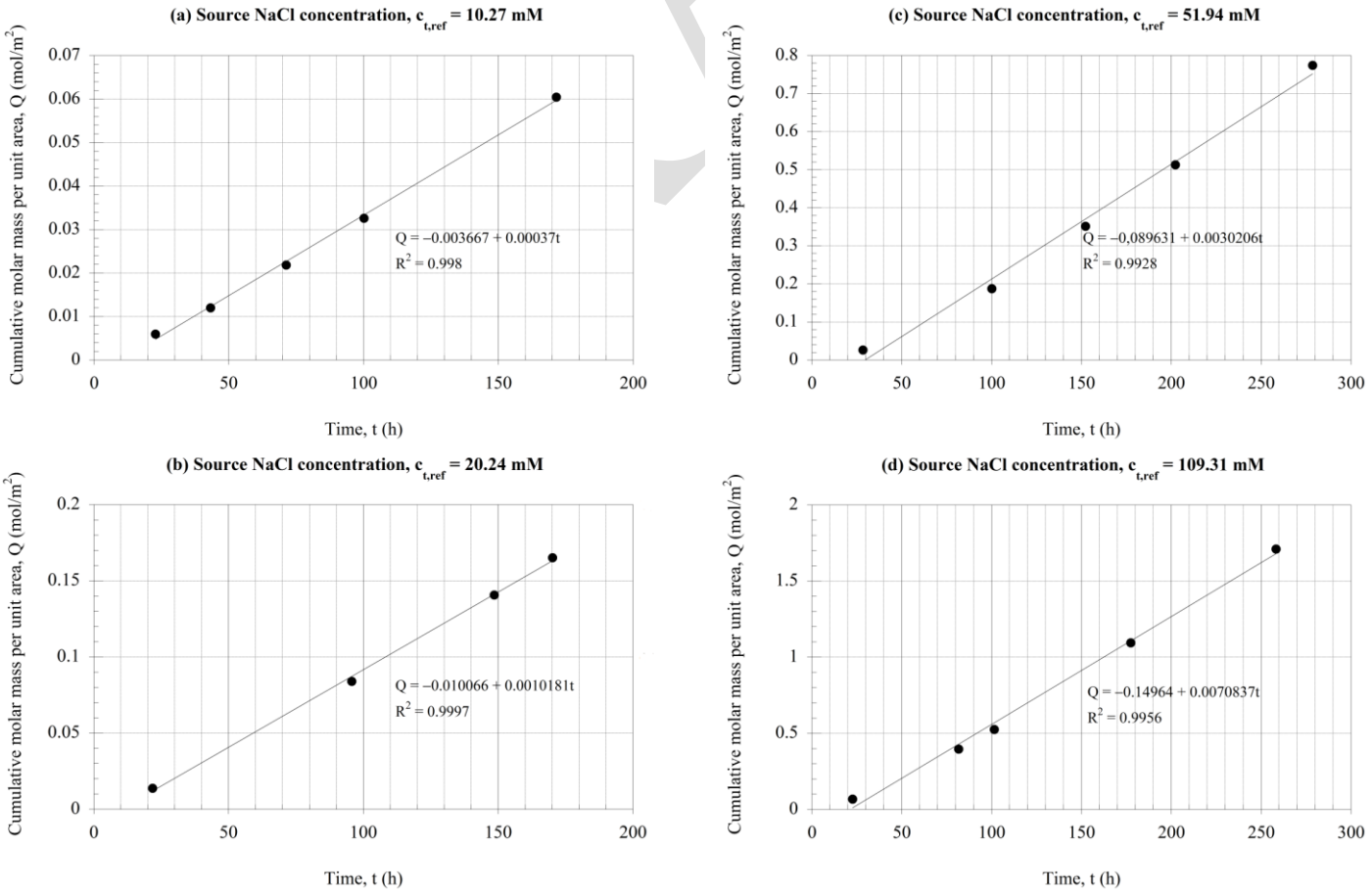

Figure 3. Cumulative molar mass of NaCl per unit area as a function of time during the multiple-stage chemico-osmotic test. (a) $c_{t,ref} = 10$ mM, (b) $c_{t,ref} = 20$ mM, (c) $c_{t,ref} = 50$ mM, (d) $c_{t,ref} = 100$ mM.

4.2 *Chemico-osmotic test on calcium bentonite*

The second chemico-osmotic test was performed on a calcium bentonite specimen, in order to analyse the osmotic behaviour of bentonite in long term landfill condition, i.e. when the cation exchange phenomenon has been developed completely and the bentonite exchange sites are entirely saturated with calcium ions.

The chemico-osmotic test was performed using the oven dried squeezed material, rehydrated with DW and then statically compacted, in a drained compaction mould, at a porosity, n, equal to 0.67. After assembling the cell, DW was circulated through the top piston and the bottom pedestal for two weeks in order to establish a steady baseline differential pressure, before a concentration gradient was applied to the specimen. A source concentration of $CaCl_2$ then was injected into the top porous stone, while DW was continuously circulated in the bottom porous stone.

A multiple-stage chemico-osmotic test was performed by sequential circulation of chemical solutions containing 5.37 and 10.40 mM $CaCl_2$ concentrations at a constant flow rate of 0.05 mL/min.

The global reflection coefficient values, ω_g, obtained during the multiple-stage chemico-osmotic test, are shown in Fig. 4 as a function of time. The ω_g values are determined using Eq. (33), on the basis of the differential pressure, Δu, measured during the test with a time step of 10 min, and the osmotic pressure, $\Delta\Pi$, calculated from the average of the top and bottom $CaCl_2$ concentrations.

The trend of the global reflection coefficient shows that a steady state has been reached for each stage. The steady state ω_g values tend to decrease as the salt concentration in the top porous stone increases. The recorded values are very low and range from 0.5%, for a 5.37 mM $CaCl_2$ source concentration, to 0.2%, for a 10.40 mM $CaCl_2$ source concentration. The global reflection coefficient can be assumed completely null for higher molarities. The results highlight that calcium bentonite shows very low osmotic behaviour at the tested molarities values.

4.3 *Swelling pressure test*

The swelling pressure test was performed using dry specimens, prepared with the squeezed oven dried bentonite and characterized by an initial dry height of 5 mm, which were allowed to swell to 10 mm during hydration. The final hydrated volume of the specimens corresponded to n = 0.81.

The test was performed by hydrating five different specimens with five different NaCl solutions, characterized by increasing concentrations, i.e. 5, 10, 20, 50 and 100 mM. After hydration, the specimen volume change was inhibited and the value of the swelling pressure was recorded after a short transitional phase.

The swelling pressure trend is reported in Fig. 5 for each test as a function of time. Since, during the tests, the load cell was unloaded until the specimen swelled to 10 mm, the initial swelling/hydration phase of the dry material (from 5 to 10 mm) was characterized by null swelling pressure values.

All the tests show that the swelling pressure increases for approximately 15-20 h, during the controlled hydration phase (i.e. when the volumetric strain is inhibited), and that the equilibrium swelling pressure is reached when the hydration phase is completed. Moreover, in the tests with lower NaCl concentrations (i.e. for 5 and 10 mM NaCl equilibrium solutions), the specimens were successively back-pressurized to 300 kPa. The obtained results show that the swelling pressure value does not change after back-pressurization.

In the test performed using the 100 mM NaCl solution, the bentonite specimen did not rise to 10 mm, as it stopped at a height of 9.5 mm, and the load cell was never loaded during the test. For this reason, the swelling pressure for this test was taken equal to zero.

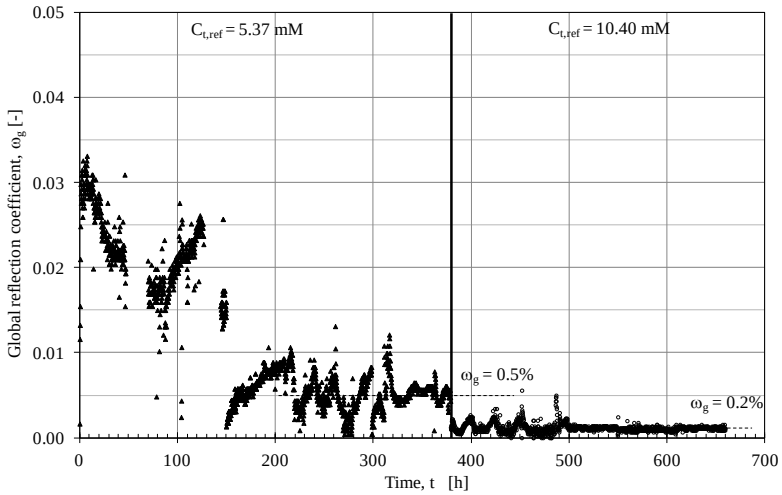

Figure 4. Global reflection coefficient as a function of time during the multiple-stage chemico-osmotic test on the calcium bentonite specimen.

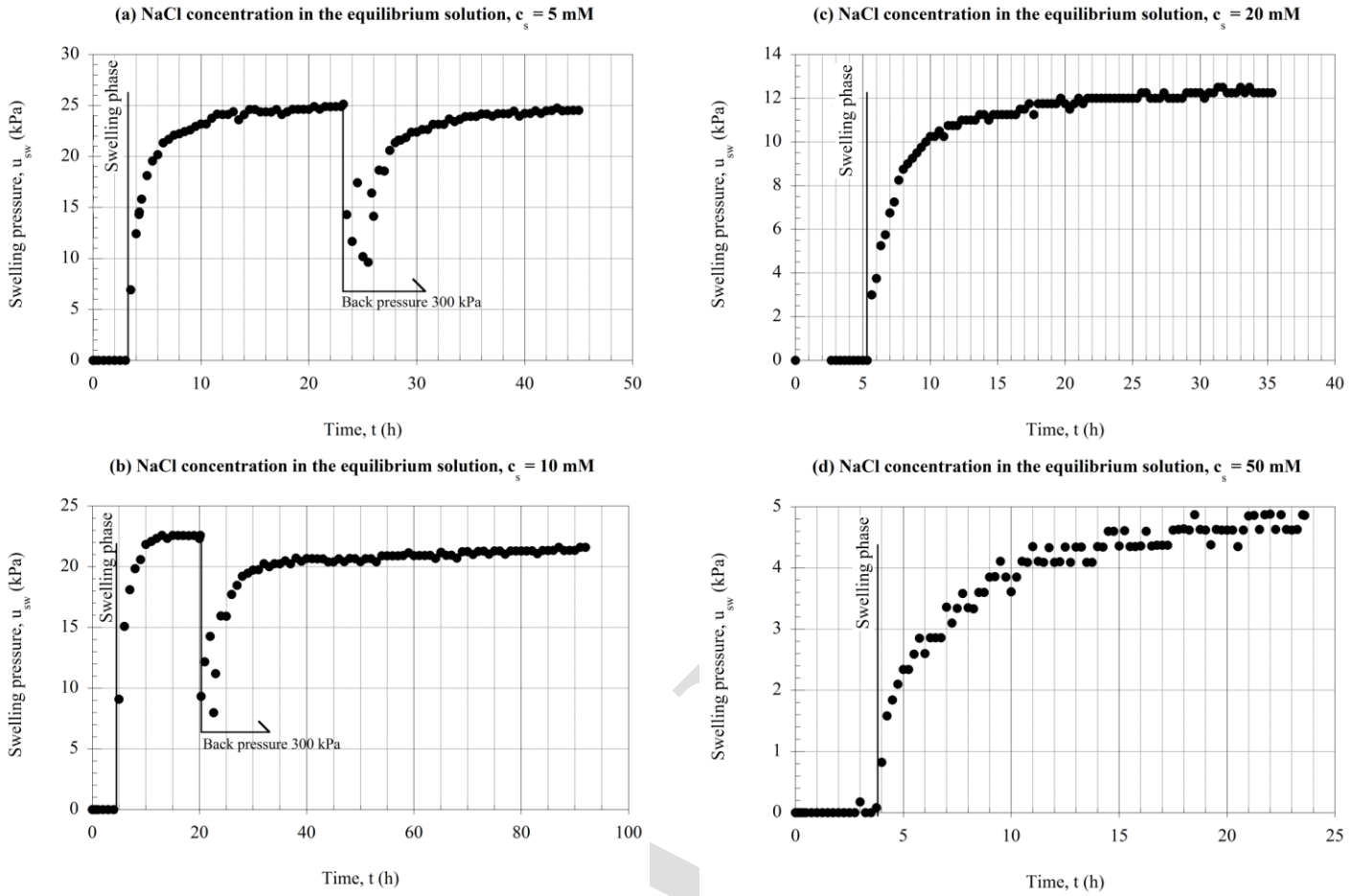

Figure 5. Swelling pressure as a function of time. (a) $c_s = 5$ mM, (b) $c_s = 10$ mM, (c) $c_s = 20$ mM, (d) $c_s = 50$ mM.

4.4 *Interpretation of the results on sodium bentonite*

The experimental results can be related to the physical and chemical properties of the tested bentonite under the assumption that the microscopic deviations of the state variables from their average values are negligible. In such a case, both the global reflection coefficient and the swelling pressure depend on the solid skeleton electric charge through Eqs. (19) and (37). Therefore, from the best fitting of the theoretical curves with the experimental data of both tests, a value of $\bar{c}_{sk,0}$ equal to 90 mM was found. Therefore, from the best fitting of the theoretical curves with the experimental data of both tests, a value of $\bar{c}_{sk,0}$ equal to 90 mM was found. The obtained theoretical curves are reported in Figs. 6 and 7, together with the experimental data.

The salt concentration at the top boundary was taken equal to $c_{t,avg}$ to determine ω_g, while the salt concentration at the bottom boundary was considered equal to zero, i.e. $c_b \cong c_{b,avg} \cong 0$. The sodium transport number was calculated from the sodium and chloride free-solution diffusion coefficient values (Shackelford and Daniel, 1991): $D_{Na,0} = 13.3 \cdot 10^{-10}$ m^2/s, $D_{Cl,0} = 20.3 \cdot 10^{-10}$ m^2/s.

In Fig. 8, the experimental reflection coefficient data were also fitted with the empirical semi-log linear curve proposed by Shackelford et al. (2003) and Malusis et al. (2003):

$$\omega_g = A + B \cdot \log(c_{t,avg}) \tag{39}$$

where A and B are the regression parameters. The value of the coefficient of determination R^2 close to one confirms the ability of this empirical curve to fit the ω_g experimental data, as it was found by Malusis et al. (2003) for the Kemper and Rollins (1966) and Malusis and Shackelford (2002a) data. However, the regression parameters A and B should be intended as functions of the soil porosity (Malusis et al., 2003) and of the bottom boundary condition (i.e. $c_{b,avg}$). The advantage of interpreting the experimental data with the proposed theoretical model is that, when the single unknown parameter, $\bar{c}_{sk,0}$, has been calibrated on a restricted experimental data set, the global reflection coefficient values can be estimated for different soil porosities and boundary conditions through Eq. (37).

The tortuosity factor was determined by plotting the measured values of $D^*_{\omega g}$ as a function of the corresponding values of the complement to 1 of ω_g, i.e. $(1-\omega_g)$ and finding the intercept of the linear regression with the ordinate axis at $(1-\omega_g) = 1$, i.e. $\omega_g = 0$ (Fig. 9). The tortuosity factor in Eq. (36) is in fact given by:

$$\tau_m = \left(\frac{D^*_{\omega g}}{D_{s,0}} \right)_{\omega_g = 0} \tag{40}$$

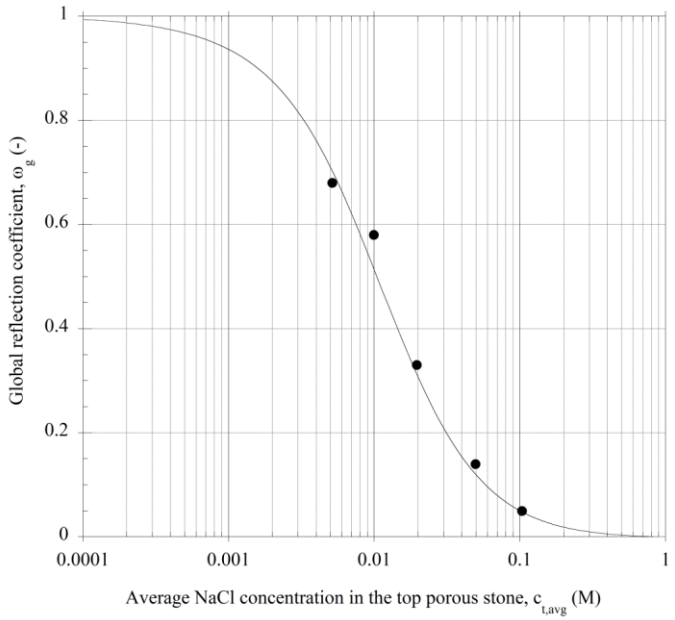

Figure 6. Global reflection coefficient, ω_g, as a function of the average NaCl concentration at the top boundary of the bentonite specimen, with the best fitting theoretical curve, obtained for $\bar{c}_{sk,0} = 90$ mM in Eq. (33) (continuous line).

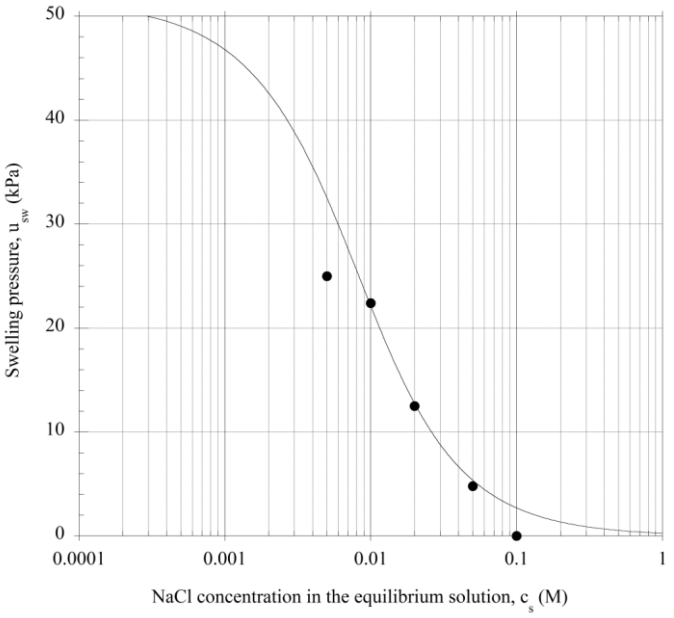

Figure 7. Swelling pressure, u_{sw}, as a function of the NaCl equilibrium concentration, with the best fitting theoretical curve, obtained for $\bar{c}_{sk,0} = 90$ mM in Eq. (19) (continuous line).

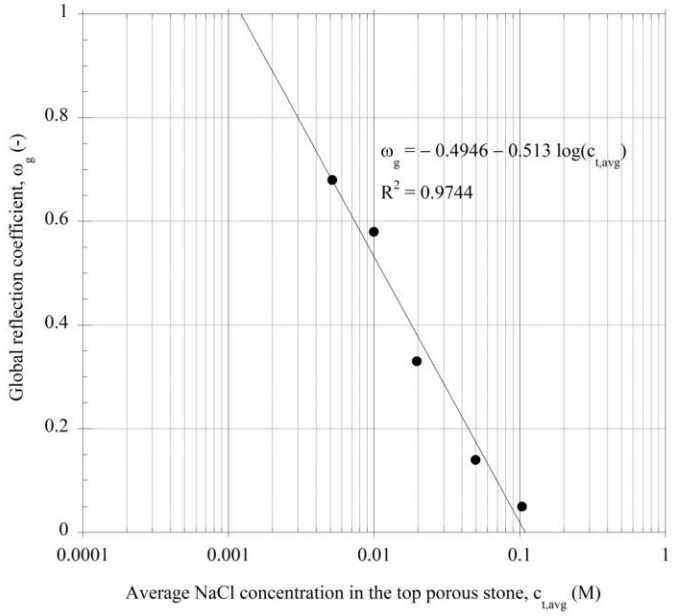

Figure 8. Semi-log linear regression of the measured global reflection coefficients versus average NaCl concentration at the top boundary of the bentonite specimen.

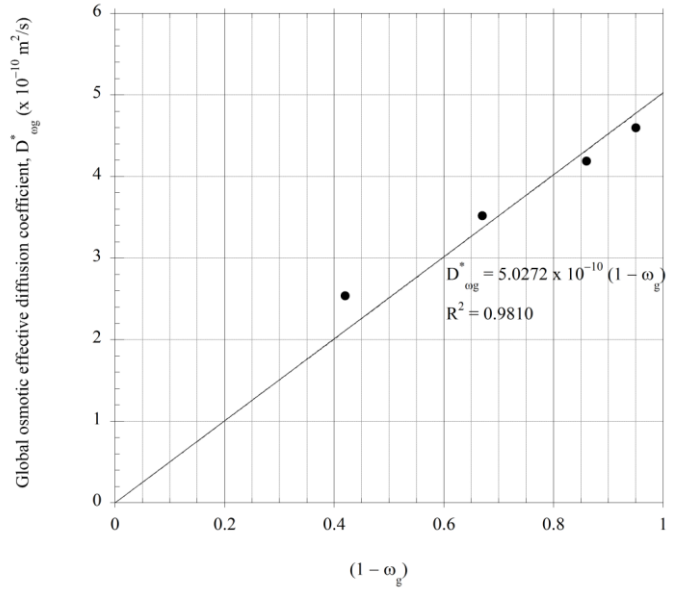

Figure 9. Global osmotic effective diffusion coefficient, $D^*_{\omega g}$, as a function of the complement to 1 of the global reflection coefficient, ω_g, with the theoretical linear relation given by Eq. (32) (continuous line).

where $D_{s,0}$ is the NaCl free solution diffusion coefficient, which is equal to (Shackelford and Daniel, 1991).

A value of τ_m equal to 0.31 was obtained from the data plotted in Fig. 8. The resulting theoretical curve of $D^*_{\omega g}$ is reported in Fig. 9 as a function of the top boundary salt concentration.

The obtained values of $\bar{c}_{sk,0}$ and τ_m are compared in Table 2 with those derived by Dominijanni and Manassero (2012b) from the interpretation of the experimental results of Malusis and Shackleford (2002a, 2002b), relative to a geosynthetic clay liner, with a bentonite porosity, n, of 0.79 for different concentrations of potassium chloride (KCl). The differences in the parameters obtained from the two studies can be attributed to both the different mineralogical compositions of the tested bentonites and the different salts contained in the pore solutions.

The theoretical linear relationship between $D^*_{\omega g}$ and $(1-\omega_g)$ in Fig. 9 is a consequence of assuming that the pore-scale variations in the hydraulic pressure, ion concentrations, and water velocity within the soil are negligible: as a result, the agreement of the experimental data with the linear relationship is an indication of the acceptability of this assumption.

Table 2. Comparison between the physical parameters derived from the interpretation of the experimental results in this work and those obtained by Dominijanni and Manassero (2012b) from the interpretation of the tests carried out by Malusis and Shackelford (2002a, 2002b).

Experimental data	This study	Malusis and Shackelford (2002a; 2002b)
Material	Natural sodium bentonite	Geosynthetic clay liner containing natural sodium bentonite
Method for removing soluble salts	Squeezing	Flushing
Tests	Chemico-osmotic test and swelling pressure test	Chemico-osmotic test
Salt in pore solution	NaCl	KCl
Porosity, n (-)	0.81	0.79-0.80
Solid skeleton charge concentration, $\bar{c}_{sk,0}$ (mM)	90	46
Tortuosity factor, τ_m (-)	0.31	0.14

The goodness of the linear fitting shown in Fig. 9 (R^2 = 0.9810) and the possibility of fitting both the global reflection coefficient and the swelling pressure data with a single value of $\bar{c}_{sk,0}$ are indications of the ability of the proposed theoretical approach to simulate the bentonite behaviour.

5 CONCLUSIONS

A theoretical approach that takes into account the interaction between the electric charge of the bentonite solid skeleton and the ions contained in the pore solution has been proposed. The phenomenological parameters introduced in this theoretical approach were measured for a bentonite specimen with porosity, n, of 0.81, over a range in sodium chloride concentration in the pore solution varying from 5 mM to 100 mM. The global reflection coefficient, ω_g, was found to decrease with an increase in the salt concentration. This result is in agreement with the trends given by the proposed theoretical model, assuming that the microscopic deviations of the pore solution state variables from their average values are negligible. If this assumption is accepted, the experimental data can be used to derive the electric charge of the solid skeleton (per unit solid volume), $\bar{c}_{sk,0}$, and the tortuosity factor, τ_m. The transport properties of bentonite can be estimated from these physical properties to evaluate its performance as a hydraulic and contaminant barrier in field applications. However, in order to verify the applicability of the proposed model under different boundary conditions and for different salts contained in the pore solution, further experimental evaluations must be conducted. Moreover, the results obtained for a single salt contained in the bentonite pore solution need to be extended to the more general problem of a solution containing an unspecified number of salts, in order to evaluate the performance of bentonites that are used as contaminant barriers for real leachates.

6 REFERENCES

Coussy, O. (2004). Poromechanics. Chichester: Wiley.

Di Emidio, G. (2010). *Hydraulic and chemico-osmotic performance of polymer treated clays.* Ph. D. Thesis., Ghent: Ghent University.

Dominijanni, A. & Manassero, M. (2012b). Modelling the swelling and osmotic properties of clay soils. Part I: The phenomenological approach. *International Journal of Engineering Science* 51, 32-50.

Dominijanni, A. & Manassero, M. (2012b). Modelling the swelling and osmotic properties of clay soils. Part II: The physical approach. *International Journal of Engineering Science* 51, 51-73.

Dominijanni, A., Manassero, M. & Puma, S. (2013). Coupled chemical-hydraulic-mechanical behaviour of bentonites: *Geotechnique* 63 (3), 191-205.

Donnan, F.G. (1911). Theorie der Membrangleichgewichte und Membranpotentiale bei Vorhandensein von nicht dialysierenden Elektrolyten. Ein Beitrag zur physikalisch-chemischen Physiologie, Zeitschrift für Elektrochemie und angewandte physikalische Chemie 17, 572-581. English translation republished in Journal of Membrane Science 100 (1995), 45-55.

Kang, J.-B. & Shackelford, C.D. (2009). Clay membrane testing using a flexible-wall cell under closed-system boundary conditions. *Applied Clay Science* 44, 43-58.

Kemper, W.D. & Rollins, J.B. (1966). Osmotic efficiency coefficients across compacted clays. *Soil Science Society of America, Proceedings* 30, 529-534.

Malusis, M.A., Shackelford, C.D. & Olsen, H.W. (2001). A laboratory apparatus to measure chemico-osmotic efficiency coefficients for clay soils. *Geotechnical Testing Journal* 24, 229-242.

Malusis, M.A. & Shackelford, C.D. (2002a). Chemico-osmotic efficiency of a geosynthetic clay liner. *Journal of Geotechnical and Geoenvironmental Engineering* 128, No. 2, 97–106.

Malusis, M.A. & Shackelford, C.D. (2002b). Coupling effects during steady-state solute diffusion through a semipermeable clay membrane. *Environmental Science and Technology* 36, No. 6, 1312–1319.

Malusis, M.A., Shackelford, C.D. & Olsen, H.W. (2003). Flow and transport through clay membrane barriers. *Engineering Geology* 70, 235-248.

Shackelford, C.D. & Daniel, D.E. (1991). Diffusion in saturated soil: I. Background. *Journal of Geotechnical Engineering*, 117, No. 3, 467–484.

Shackelford, C.D. & Lee, J.-M. (2003). The destructive role of diffusion on clay membrane behavior. *Clays and Clay Minerals* 51, No. 2, 186–196.

Yeo, S.-S., Shackelford, C.D. & Evans, J.C. (2005). Membrane behaviour of model soil-bentonite backfill mixtures. *Journal of Geotechnical and Geoenvironmental Engineering* 131, No. 4, 418-429.